Journal of Biomolecular Structure and Dynamics

ISSN: (Print) (Online) Journal homepage: https://www.tandfonline.com/loi/tbsd20

Use of simplified models for theoretical prediction of the interactions between available antibodies and the receptor-binding domain of SARS-CoV-2 spike protein

G. A. Huerta-Miranda, W. I. García-García, A. Vidal-Limon & M. Miranda-Hernández

To cite this article: G. A. Huerta-Miranda, W. I. García-García, A. Vidal-Limon & M. Miranda-Hernández (2021): Use of simplified models for theoretical prediction of the interactions between available antibodies and the receptor-binding domain of SARS-CoV-2 spike protein, Journal of Biomolecular Structure and Dynamics, DOI: 10.1080/07391102.2021.2019123

To link to this article: https://doi.org/10.1080/07391102.2021.2019123

View supplementary material

Published online: 22 Dec 2021.

Submit your article to this journal

Article views: 81

View related articles

View Crossmark data

Full Terms & Conditions of access and use can be found at
https://www.tandfonline.com/action/journalInformation?journalCode=tbsd20

JOURNAL OF BIOMOLECULAR STRUCTURE AND DYNAMICS
https://doi.org/10.1080/07391102.2021.2019123

Taylor & Francis
Taylor & Francis Group

Check for updates

Use of simplified models for theoretical prediction of the interactions between available antibodies and the receptor-binding domain of SARS-CoV-2 spike protein

G. A. Huerta-Miranda, W. I. García-García, A. Vidal-Limon and M. Miranda-Hernández

Instituto de Energías Renovables, Universidad Nacional Autónoma de México, Temixco, Morelos, México

Communicated by Ramaswamy H. Sarma.

ABSTRACT

The negative impact of infectious diseases like COVID-19 on public health and the global economy is evident. This pandemic represents a significant challenge for the scientific community to develop new practical analytical methods for accurately diagnosing emerging cases. Due to their selectivity and sensitivity, new methodologies based on antigen/antibody interactions to detect COVID-19 biomarkers are necessary. In this context, the theoretical, computational modeling reduces experimental efforts and saves resources for rational biosensor design. This study proposes using molecular dynamics to predict the interactions between the Receptor Binding Domain (RBD) of the SARS-CoV-2 spike protein simplified model and a set of highly characterized antibodies. The binding free energy of the antigen/antibody complexes was calculated for the simplified models and compared against the complete SARS-CoV-2 ectodomain to validate the methodology. The structural data derived from our molecular dynamics and end-point free energy calculations showed a positive correlation between both approximations, with a 0.82 Pearson correlation coefficient; $t = 3.661$, df = 3, p-value = 0.03522, with a 95% confident interval. Furthermore, we identified the interfacial residues that could generate covalent bonds with a specific chemical surface without perturbing the binding dynamics to develop highly sensitive and specific diagnostic devices.

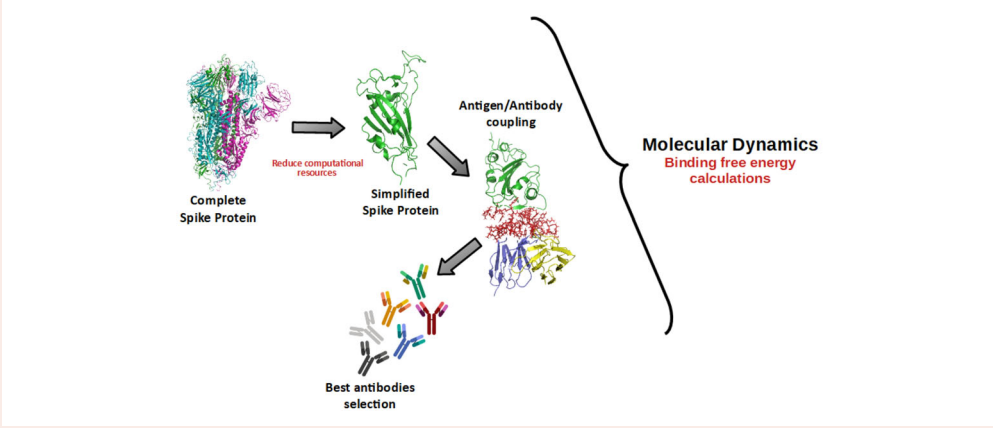

Abbreviations: Fab: Fragment Antibody; GAMD: Gaussian Accelerated Molecular Dynamics; RBD: Receptor Binding Domain; SP-1: Spike Protein 1; SARS-CoV-1: SP-2, Spike protein SARS-CoV-2

ARTICLE HISTORY
Received 21 July 2021
Accepted 2 December 2021

KEYWORDS
Simplified models; COVID-19; SARS-CoV-2; molecular dynamics; binding free energy

1. Introduction

The recent highly pathogenic SARS-CoV-2 coronavirus outbreak towards the end of 2019 (C. Wang et al., 2020; Zhou et al., 2020a) has caused a global public health emergency with almost two hundred million confirmed infections and more than four million deaths worldwide (World Health Organization, 2020). Early detection of the infection has been a challenging task, and accurate data acquisition on the spread and infectivity of the virus is essential for the population diagnosis and adequate distribution of government resources to provide an effective solution to the pandemic. To achieve that, we depend on synergy among various areas of science.

The current widely used technique to detect SARS-CoV-2 is the quantitative reverse transcription-polymerase chain

CONTACT A. Vidal-Limon avl@ier.unam.mx; M. Miranda-Hernández mmh@ier.unam.mx

Supplemental data for this article can be accessed online at http://dx.doi.org/10.1080/07391102.2021.2019123

© 2021 Informa UK Limited, trading as Taylor & Francis Group

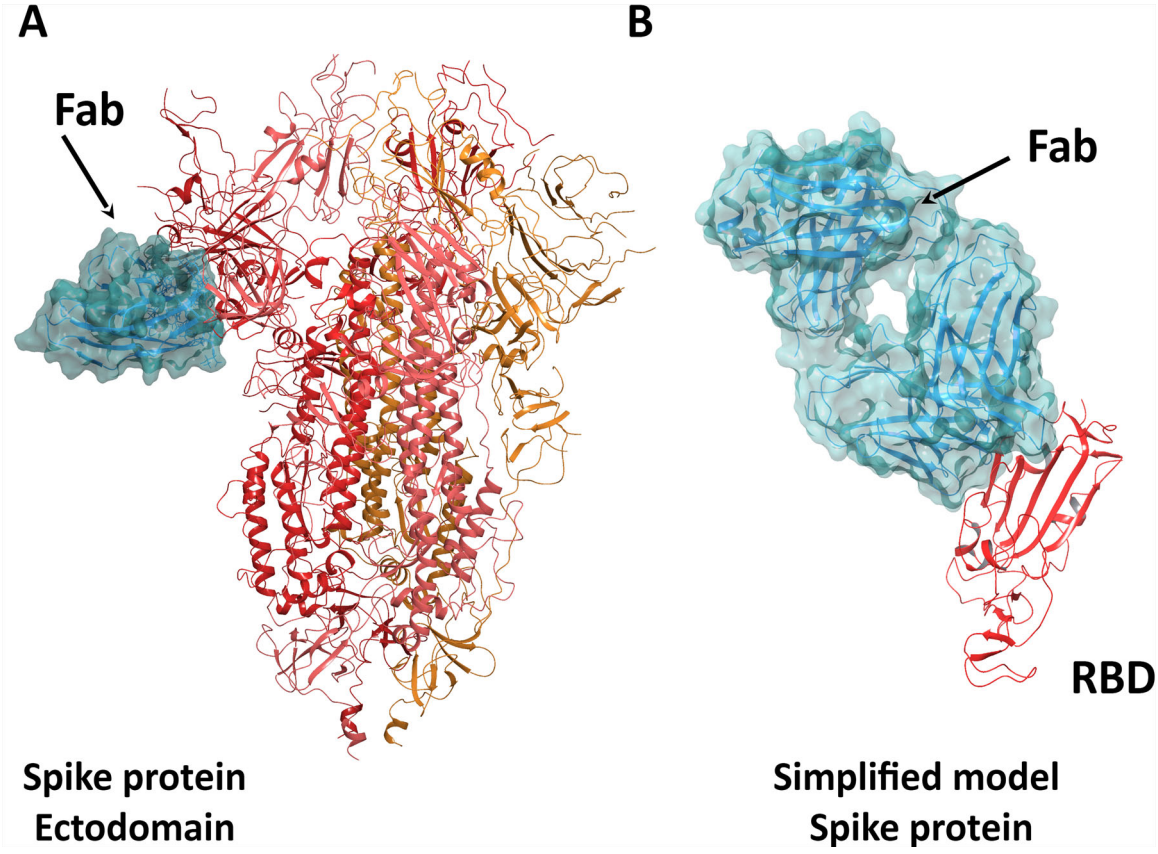

Figure 1. Complete and simplified model of the SP spike proteins of the SARS-CoV-2 virus. A. The complete ectodomain of SP-2, considering the transmembrane region. B. Simplified model of SP-2, regarding the crystal structure 6YOR and a fragment antibody.

reaction (qRT-PCR) (Chu et al., 2020; Corman et al., 2020). This technique requires trained staff, intense standardization work, and specialized equipment, making it challenging to implement in remote places or developing countries. Also, early symptoms in COVID-19 patients are not deterministic due to asymptomatic carriers and the similarity with other respiratory infections such as influenza (Won et al., 2020). Therefore, highly sensitive and specific diagnostic methods are essential in distinguishing and controlling new COVID-19 cases (Zhu et al., 2020; Zuo et al., 2017).

For adequate COVID-19 detection, selecting a biochemical indicator must be accurate (Carter et al., 2020). Some working groups have targeted efforts to isolate neutralizing-SARS-CoV-2 antibodies (Fab) from convalescent individuals. However, recent reports on variants from India indicate that new strains are resistant to neutralization with these produced antibodies from convalescent individuals and insensitive to monoclonal antibodies derived from vaccination (Planas et al., 2021). Therefore, the quick identification of reactive antibodies is a relevant theme in mitigating nowadays global pandemic.

Fabs could be used as scaffolds for the design and development of biosensor technologies (Huo et al., 2020; Ju et al., 2020; Pinto et al., 2020). A typical target of such antibodies is the viral Spike Protein (SP), a trimeric complex of ~20 nm in length, which binds to the angiotensin-converting enzyme 2 (ACE2) in human host cells (see Figure 1A) (Hoffmann et al., 2020; Walls et al., 2020; Q. Wang et al., 2020; Wrapp et al., 2020; Zhou et al., 2020b).

The SP proteins contain two subunits: the S1 subunit contains two main structural elements, the receptor-binding domain (RBD) and the N-terminal domain (NTD). The S2 subunit is responsible for the virus-cell membrane fusion after the RBD domain activates the ACE2 receptor (Hoffmann et al., 2020). There are various reports about the binding capacity of different antibodies capable of neutralizing the RBD domain (Huo et al., 2020; Walls et al., 2020). In these studies, since the RBD is a critical factor to determine the tropism and infectivity of SARS-CoV-2, the neutralization of SP protein is the primary goal to prevent and control the spread of the disease (Hoffmann et al., 2020; Souza et al., 2020; Walls et al., 2020). Unfortunately, recent clinical reports argue that inmuno-detections methods for SARS-CoV-2 spike protein showed cross-reactions against Dengue virus (Henrina et al., 2020; Lustig et al., 2021; Masyeni et al., 2021; Quental et al., 2021; Santoso et al., 2021); the clinical challenge is a current topic among medical and scientific communities to provide accurate diagnosis and treatment (Bicudo et al., 2020).

Compiling the available information about the previously mentioned protein-protein interactions, we propose using molecular dynamics techniques on simplified models to predict antibody-antigen interaction between the RBD domain and available antibodies. These methods are necessary to reduce time and computational resources in understanding systems where many molecular interactions are involved (Forssen et al., 2020; Jarocka et al., 2014; Urban, 2000). Our working group has contributed to the elucidation and description of bioelectrochemical interfaces assisted by

molecular dynamics simulations (Vidal-Limon et al., 2021) and the influence of an electrical field in the behavior of rotavirus VP6 protein coupled on a current collector (Garcia-Garcia et al., 2019). We aim to use molecular dynamics and end-point free energy calculations on specific and reported antibodies, optimize the algorithms and restrict the calculations to the atoms involved in the molecular interactions. This work describes the binding free energy between selected antibodies and the complete trimeric structures of SARS-CoV-1 (SP-1), SARS-CoV-2 (SP-2) spike protein ectodomain, and the SP-2 simplified model (see Figure 1B). We looked for similar tendencies and correlations between the whole and simplified systems. The validation of our methodology includes using the Fab S230 antibody, previously described for SP-1 as a negative control. The complete and simplified models of SP-2 showed similar behavior when Fab S230 was present in the simulation.

Moreover, the linear correlation between the binding free energy of complete and simplified models showed a Pearson coefficient of 0.82, suggesting that simplified models reproduce the behavior of the complete ectodomain. It is important to outline that using whole viral structure models to describe full dynamics and interactions (Casalino et al., 2021) may be challenging in computational cost, mostly in developing countries. Thus, herein we propose an alternative methodology to achieve similar results in significantly less computation time.

2. Methods and computational tools

2.1. Construction and refinement of three-dimensional models of available spike proteins and antibodies

The protein structures corresponding to the complete spike proteins of the SARS-CoV-2 in complex with well-known antibodies (PDB 6XEY (Liu et al., 2020), 6XCN (Barnes et al., 2020)) and simplified structure of SARS-CoV-2 (PDB 6YOR (Huo et al., 2020)) were taken from the PDB database (RCSB Protein Data Bank). Spike protein of the SARS-CoV-1 virus in complex with Fab S230 (PDB 6NB6 (Walls et al., 2019)) was also simulated. The SP structures and antibodies were prepared with the routine '*Protein Preparation Wizard*' (Schrödinger Maestro v. 2019-4) to avoid steric hindrances and identify missing atoms. The selection of the antibodies considers the most extensively studied and representative structures available in the literature. The protonation states of the amino acid residues of the studied proteins were analyzed with the *PropKa* routine (Olsson et al., 2011) and maintained at pH 7. Finally, 75 Å cubic systems fully solvated with TIP3P waters were built to contain the complete systems (trimers-antibody) and neutralized with Na^+ or Cl^- counterions. The models were built with the *tleap* tool of Ambertools19 from the Amber18 software package using ff14SB, ff19SB, GAFF, and Glycam forcefields (Case et al., 2018).

2.2. Accelerated molecular simulation and free energy calculations

The models mentioned above were simulated with Gaussian accelerated molecular dynamics (GaMD) (Miao et al., 2015; Miao & McCammon, 2017), which describes and reweight potential energy hypersurfaces by adding boost potentials to the potential energy and dihedral angles. Both systems were minimized for 10,000 steps with the Conjugated Gradient-Steepest descent mixed algorithm and heated for 5 ns of molecular dynamics under NPT collective with integration times of 1 fs. After that, both systems were pre-equilibrated for 50 ns in NPT with integration times of 2 fs. The complete systems were simulated along 100 ns with an integration time step of 2 fs. In contrast, the simplified models were simulated in triplicate for 500 ns. A dual acceleration scheme imposed by Gaussian flooded potentials on total potential energy and dihedral was applied to complexes to evaluate conformational changes during simulations.

The antibody-antigen free binding energy for each complex was calculated by the MM/GBSA method using an implicit solvent model to recover the contribution of each residue to the formation of the antibody-SP-2 complex. Two rounds of calculations were performed: 1) the complete systems during all frames and 2) the simplified models during all frames of the production of accelerated molecular dynamics.

The MM/GBSA method (molecular mechanics combined with the Poisson-Boltzmann or Generalized method of continuous solvation) has been widely used to estimate binding affinities to the ligand in many systems.

The free energy of a state is estimated from the following sum:

$$\Delta G = E_{bind} + E_{ele} + E_{vdw} + G_{pol} + G_{gas} - TS \quad (1)$$

Where, the first three terms are MM energy terms from bonding (bond, angle, and dihedrons), electrostatic, and Van der Waals interactions. G_{pol} and G_{gas} are the polar and non-polar contributions to the free solvation energies. G_{pol} is typically obtained by solving the PB equation or using the generalized Born model (GB, which provides the MM/GBSA approach). At the same time, the non-polar term is estimated from a linear relationship with solvent-accessible surface area (SASA). The last term in the equation is the temperature (T) at 298 K, multiplied by entropy (S). The dielectric constants for the solvent and solute were set to 80 and 5, respectively (Genheden & Ryde, 2012, 2015). The calculations were carried out with the Amber18 CUDA version software package and *cpptraj* program (Roe & Cheatham, 2013). All graphics were prepared with R Statistical package v. 4.0.1.

3. Results and discussion

3.1. Design of simplified model: Structural comparison between complete and simplified systems

The intermolecular interactions between a set of proteins conforming protein-protein complexes are governed by various physicochemical properties that determine the affinity between the components. To describe all the forces involved in the interaction between the spike proteins SP-1 and SP-2, corresponding to the SARS-CoV-1 and SARS-CoV-2, respectively, we simulated by molecular dynamics the complete models from the available PDB crystal structures.

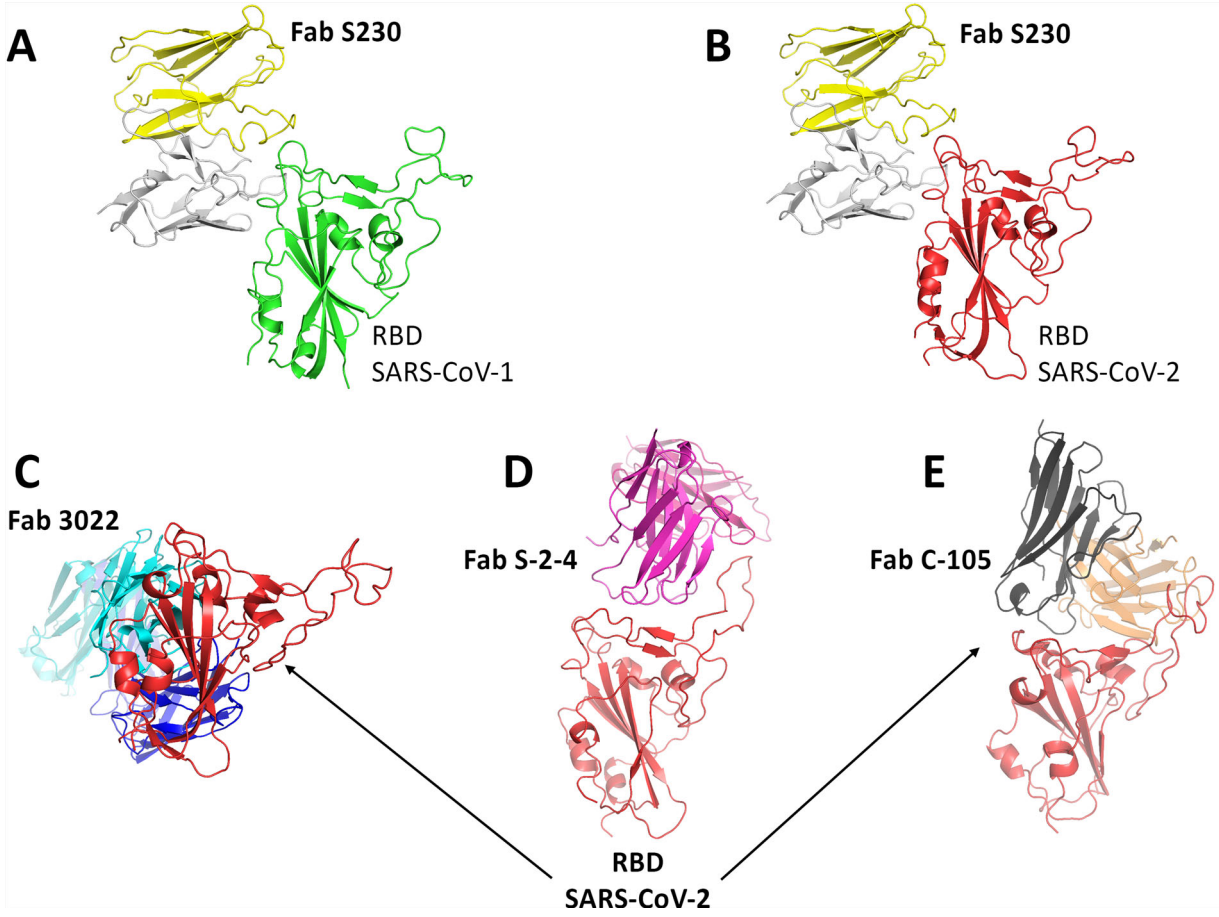

Figure 2. RBD Simplified models in complex with different fragment antibodies. A. SP1-Fab S230. B. SP2-Fab S230. C. SP2-Fab 3022. D. SP2-Fab S-2-4. E. SP2-Fab C105.

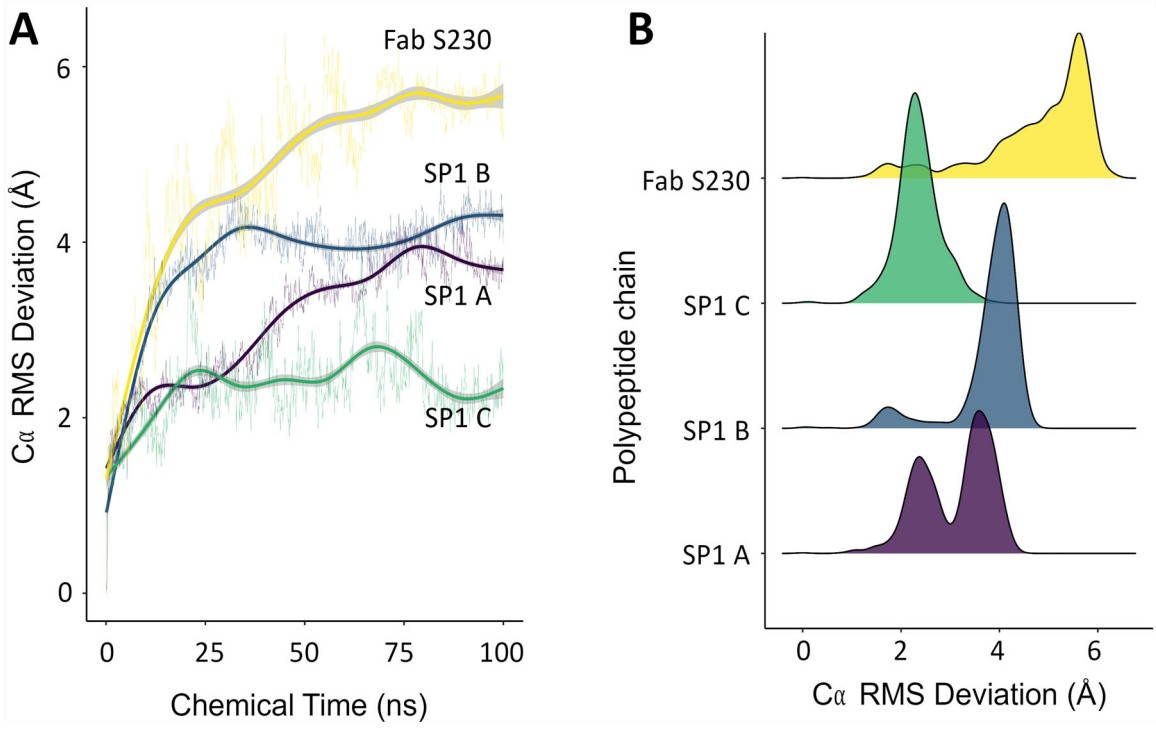

Figure 3. RMS Deviations of complete Spike Protein model along 100 ns of simulation. A. Ca RMS Deviation of SP-1 – Fab S230 (PDB: 6NB6) all atoms. B. RMS Deviation distribution of SP-1 – Fab S230 all atoms.

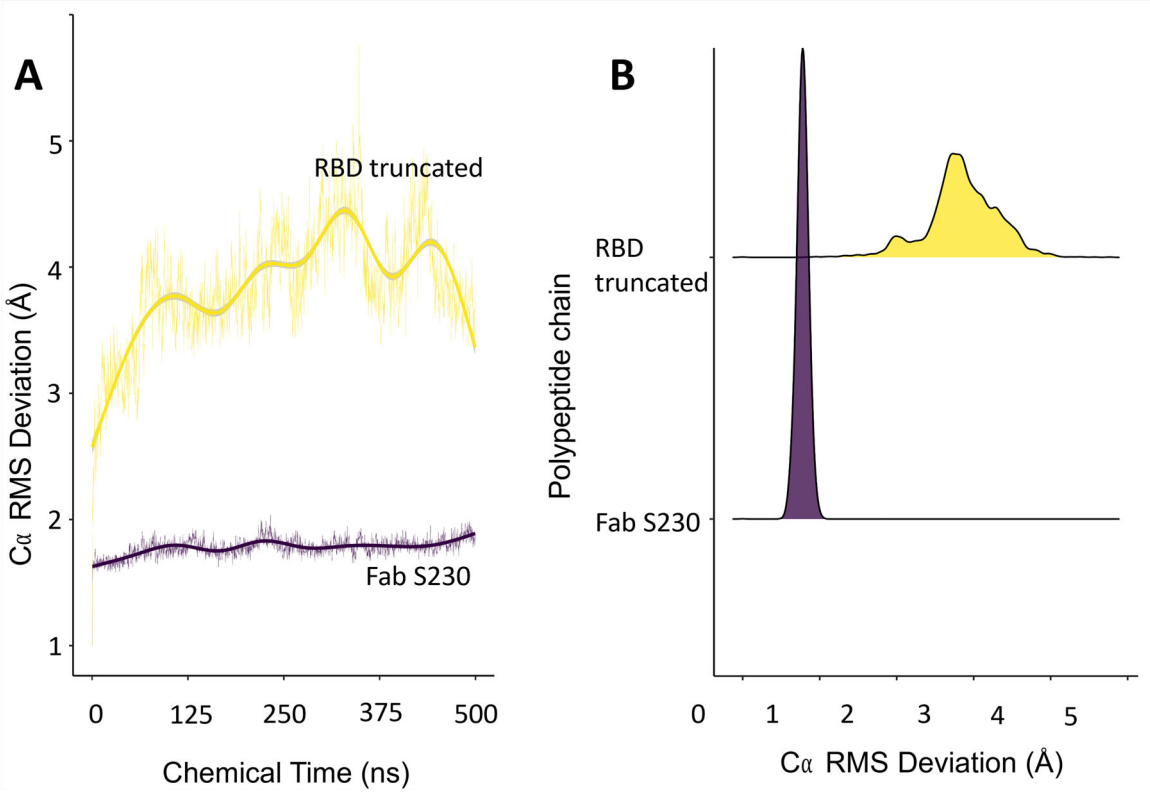

Figure 4. RMS Deviation of SP-1 – S 230 simplified model along 500 ns simulation. A. Ca RMS Deviation of SP-1 – S 230 RBD simplified model. B. RMS Deviation distribution of the simplified model.

For the SP-1 protein, the crystal model contained a dimer of the Fab S230, which shows interaction with the RBD in the open state configuration. This same antibody was tested against SP-2. Figure 2A–B shows the simplified models of SP-1 and SP-2 with the Fab S230, and Figure 2C–E shows the simplified SP-2 protein modeled with different antibody fragments.

The protein simulation of complete and simplified models allowed the calculations of changes in atomic position, speed, and acceleration. The calculated RMSD for the complete model of SP-1 – Fab S230 show similar mean values between the three subunits of SP-1, ranging between 2 and 4 Å, while the average values for the Fab S230 increase up to 6 Å in during the simulation due to the transient interaction with the RBD domain (Figure 3A–B).

The calculated RMSD of the simplified model of SP-1 – Fab S230 showed a slight increase in the atomic positions of the RBD domain of the SP-1 protein compared to Fab S230 (Figure 4). This result may be due to the 10% representation of the whole structure of SP-1 RBD ectodomain (only 197 amino acid residues, in contrast to the 1133 amino acid residues of the complete system). The ectodomain structure is assembled in the form of a trimer, providing mechanical support for the exposure of the RBD in the open state configuration; and the interdomain interactions between the connecting and transmembrane domains for the anchoring to the viral membrane. These results indicate that the simplified model preserves the structure and dynamics of the exposed residues of the RBD domain and could be used as an initial model to understand the intermolecular forces that control the virus-antibody interaction. Additionally, in the supporting material, we report the RMS deviations of the complete and simplified model of the complexes SP-2 – Fab 3022. RMSD values of the three subunits of SP-2 (Figure S1) are between 4 and 6 Å. In the case of the simplified model of SP-2, the calculated RMSD showed similar values as Fab 3022.

3.2. Free energy calculations of antigen-antibody interactions

In several reports, structures from long-term simulations are commonly used since the atoms in the system had the time to equilibrate with solvent and surrounding ions (Genheden & Ryde, 2012). In the equilibration process, the water molecules, ions, and molecular partners couple their motions resulting in lower RMSD and potential energy. In this manner, an equilibrated system results in less energy and coordinate fluctuations during the theoretical thermodynamic cycle of the end-point free energy calculations. Recent work in SARS-CoV-2 spike protein dynamics, in the microsecond time scale, demonstrated that long simulations reflect the dynamic behavior of the viral protein on its interaction with ACE2 receptor (Casalino et al., 2021), although the complexity of the whole viral protein and complete membrane section of ACE2 receptor.

The homology models available on the CHARMM-GUI server (Jo et al., 2008; Woo et al., 2020) allowed us to analyze the interaction between antibodies and SP-2 protein systems. These systems use the 6NB6 crystal of the SP-1 trimer as a

Table 1. Energy terms decomposition of the complete SP-1 and SP-2 ectodomain systems in complex with different antibodies.

	Energy Terms (Kcal · mol^{-1})*							
Complex	VdW	Elec	GB	Surf	ΔG Gas	ΔG Solv	ΔG Total	ΔΔG
SP-1 – Fab S230	−157.33 ± 12.41	−440.22 ± 60.14	550.10 ± 56.45	−22.49 ± 1.83	−597.55 ± 76.89	−22.49 ± 5.25	−69.94 ± 6.97	–
SP-2 – Fab S230	−65.13 ± 16.90	−167.65 ± 58.74	233.12 ± 50.23	−3.05 ± 0.98	−283.11 ± 65.53	212.79 ± 49.87	−23.38 ± 2.45	46.56
SP-2 – Fab 3022	−101.68 ± 31.41	−289.68 ± 130.63	325.81 ± 95.80	−14.068 ± 2.88	−391.58 ± 128.77	311.74 ± 94.37	−89.83 ± 3.64	−19.89
SP-2 – Fab S-2-4	−339.40 ± 23.93	−721.36 ± 139.10	936.21 ± 118.25	−45.54 ± 2.62	−1060.77 ± 141.50	890.67 ± 116.91	−170.10 ± 15.55	−100.16
SP-2 – Fab C105	−298.01 ± 24.01	−622.89 ± 138.92	868.78 ± 118.01	−40.10 ± 2.60	−999.91 ± 141.42	833.68 ± 116.67	−138.88 ± 4.66	−68.94

*Mean values in Kcal · mol^{-1}.

Table 2. Analysis of the energy terms of the simplified models SP-1 and SP-2 in complex with their respective antibodies.

	Energy Terms(Kcal · mol^{-1})*							
Complex	VdW	Elec	GB	Surf	ΔG Gas	ΔG Solv	ΔG Total	ΔΔG
SP-1 – Fab S230	−180.40 ± 21.44	−321.47 ± 23.27	327.33 ± 136.22	−26.70 ± 2.31	−459.39 ± 155.85	346.11 ± 89.37	−136.16 ± 37.58	–
SP-2 – Fab S230	−146.71 ± 28.44	−170.97 ± 41.94	176.36 ± 28.99	−20.75 ± 1.12	−64.68 ± 4.69	111.88 ± 28.41	−82.80 ± 33.22	53.36
SP-2 – Fab 3022	−193.75 ± 83.65	−522.75 ± 9.65	475.89 ± 110.49	−26.45 ± 11.98	−667.02 ± 221.73	447.98 ± 98.55	−305.16 ± 22.65	−168.99
SP-2 – Fab S-2-4	−339.01 ± 20.86	−722.89 ± 86.54	938.78 ± 89.87	−45.10 ± 3.25	−1061.91 ± 99.12	893.68 ± 87.33	−368.23 ± 16.88	−232.07
SP-2 – Fab C105	−319.22 ± 26.14	−286.50 ± 13.42	−376.08 ± 11.76	122.89 ± 2.05	−318.43 ± 13.30	−363.7 ± 11.72	−345.81 ± 6.46	−209.65

*Mean values are expressed in Kcal · mol^{-1} for three independent replicas.

template and incorporate the carbohydrates that generate the particular glycosylation pattern of the SP-2 proteins. This complete SP-2 system was modeled with Fab 3022 at 3 Å of distance from the RBD domain with additional 100 ns of GaMD calculated under the same conditions described above. Furthermore, to compare the results among the simplified models, a simplified model of the RBD domain of SP-1 was constructed, and the free binding energies between the corresponding models were calculated.

Free binding energy calculations were performed with MM/GBSA implicit solvent methods to pick up highly selective antibodies for the SP-2 proteins of the SARS-CoV-2 virus. From the trajectories of the complete SP-1 and SP-2 systems, various energetic terms representing the intermolecular forces acting during the coupling of the antibodies were calculated.

The predominant interactions in the complete systems are the electrostatic interactions between charged amino acids (Arg-Asp). Also, some residues can form hydrogen bonds with the nearby amino acids of the antibodies or with the solvent (see Table 1). The resulting free energies of the complete systems are in good agreement with experimental data. It has been demonstrated that the Fab S230 for SP-1 is not selective for SP-2, whereas Fab S-2-4 and Fab C105 are the most specific and highly selective against SP-2. The available antibody structures selected for this study showed a consensus binding mode, where the Fab is coupled to the RBD domain of SP-2.

Since the binding mode is shared between all the Fab available structures, we propose simplified models, with a significantly smaller atom amount than the complete system, as probe models that reproduce the tendency in the free energies of complete systems. Analysis of the MM/GBSA calculations on simplified models showed that interactions were overestimated for all terms, resulting in lower ΔG values. This result may be due to the estimation of solvent interactions, which imposes the main barrier to binding since desolvation represents the displacement of solvent molecules from the interaction site. The interaction of RBD with all the Fab was overestimated by ∼2 fold. Additionally, there was

Table 3. MM/GBSA residue decomposition of SP-2 simplified model complexes.

SP-2 – Fab 3022 complex	
Residues	Free energy (Kcal·mol^{-1})
Val 282	−1.13 ± 1.0
Lys 378	−3.28 ± 5.5
Tyr 380	−1.52 ± 1.4
Gly 381	−1.43 ± 0.8
Lys 386	−4.79 ± 1.2
Leu 390	−1.40 ± 0.6
SP-2 – Fab S-2-4 complex	
Residues	Free energy (Kcal·mol^{-1})
Tyr 380	−1.60 ± 1.57
Arg 403	−2.01 ± 1.29
Asp 405	−1.61 ± 0.12
Glu 406	−0.50 ± 0.07
Lys 417	−5.29 ± 1.46
Arg 457	−1.46 ± 0.63

*Mean values are expressed in Kcal · mol^{-1} for each residue from three independent replicas.

an increase in the local flexibility of RBD and non-restricted movement of terminal residues due to lacking anchoring protein, which is critical for the desolvation process (Table 2).

In comparison to *in vitro* systems, if the Gibbs free energy (ΔG) represents the free energy of binding and K_a and K_d are the constants of association-dissociation of the receptor/ligand complex in equilibrium:

$$\Delta G = -RT\ln K_a = RT\ln K_d \quad (2)$$

When we compare the energy of 2 binders (Fab S230 and Fab 3022) to their receptor:

$$\Delta G_1 = RT\ln K_{d1}, \Delta G_2 = RT\ln K_{d2} \quad (3)$$

Hence:

$$\Delta\Delta G = \Delta G_2 - \Delta G_1 = RT\ln(K_{d2}/K_{d1}) \quad (4)$$

For example, when $\Delta\Delta G = 1$ Kcal·mol^{-1}y $T = 298.15$ K:

$$K_{d2}/K_{d1} = 5.4 \quad (5)$$

So, if ΔG2 – ΔG1 = 1 Kcal·mol^{-1}, it means that the binder 2 is weaker than the binding energy of binder 1, then the dissociation constant of binder 2 (K_{d2}) is ∼5 times higher and of less affinity than that of binder 1 (K_{d1}). In general, at

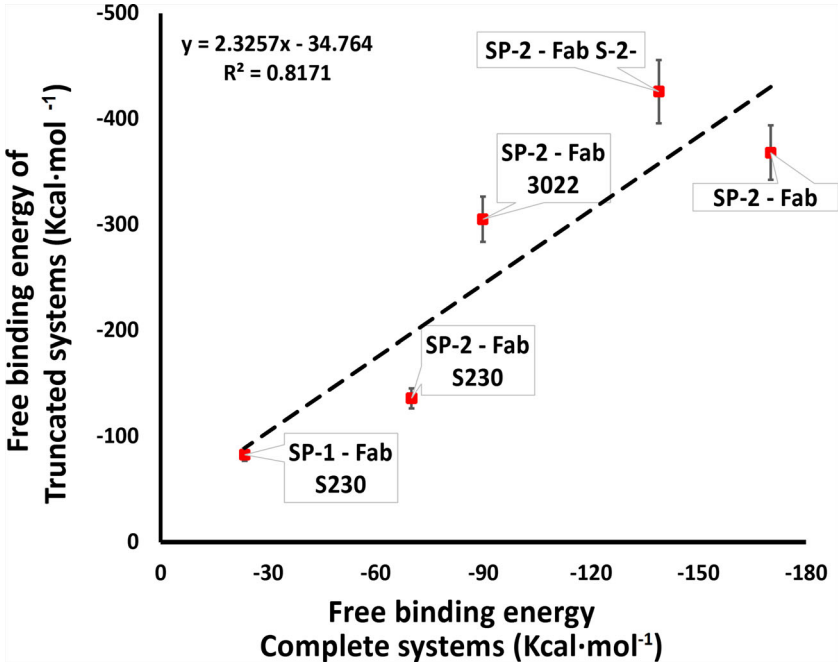

Figure 5. Linear correlation between Free energy of binding of complete and simplified models of RBD SP-2 SARS-CoV-2. Data sets were probed with a two-sided Pearson correlation analysis (Pearson correlation analysis, 95% confident interval, and *p*-value= 0. 03522).

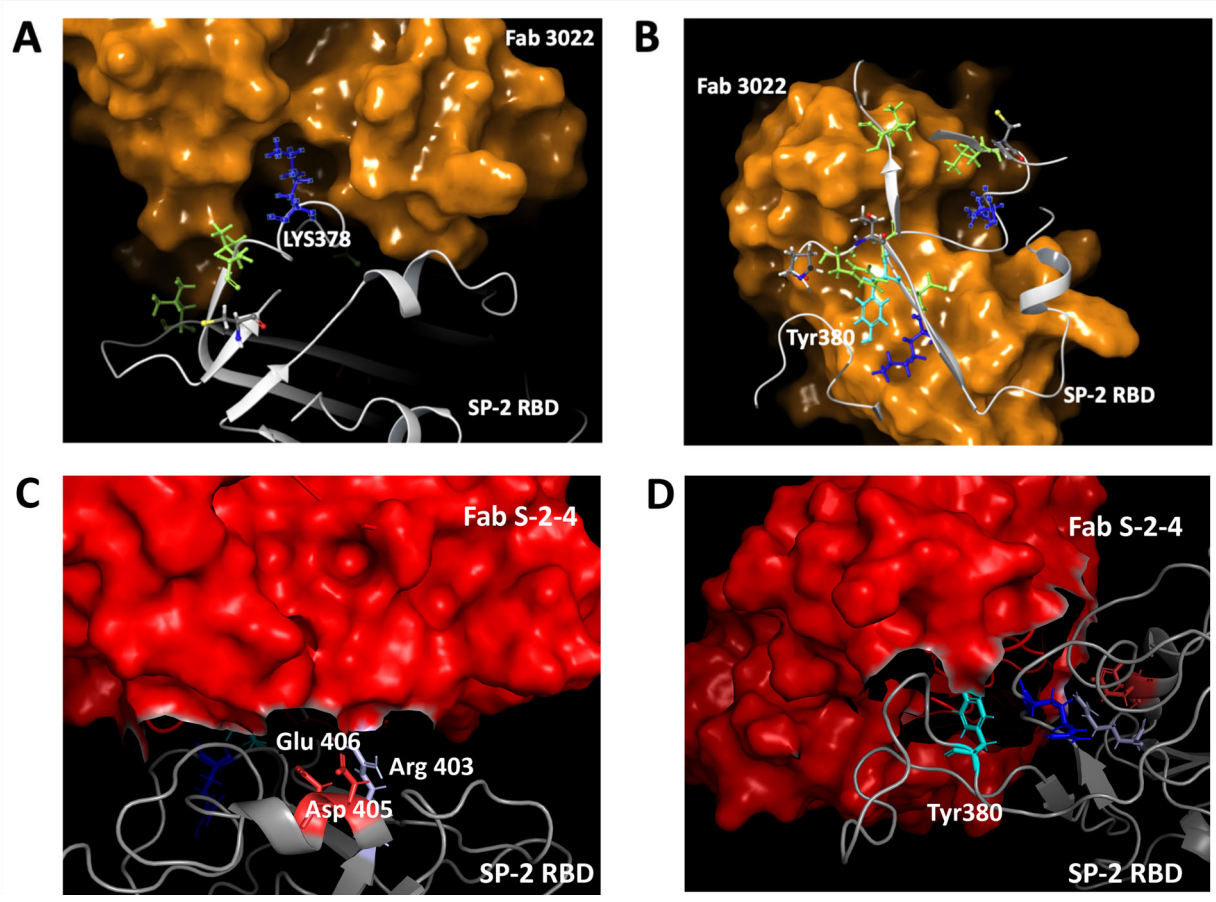

Figure 6. SP-2 – Fab interface residues. A. SP-2 Lys378 region interacting with Fab 3022. B. SP-2 Tyr380 regions with Fab 3022.C. SP-2 Acidic patch and Fab S-2-4. D. SP-2 Tyr380 and Fab S-2-4 interaction. Both Fab 3022 and Fab S-2-4 structures are depicted as orange or red solvent-accessible surfaces, respectively.

25 °C (298 K), if the value of $\Delta\Delta G = 1.4$ Kcal • mol^{-1}, it would correspond to a difference of 10 times in K_d. However, it would be necessary to calculate the free energy of dissociation in both complexes to estimate the value of K_{d2}/K_{d1} and compare it with experimental data.

For the complete systems, we found a difference of −44 Kcal • mol^{-1} between SP-1/SP-2 vs. Fab S230, which would represent a high affinity for the antibody S230, which is not specific for SP-2 RBD (ΔΔG Table 1). Moreover, the difference between SP-1 – Fab S230 and SP-2 – Fab S-2-4 complexes showed the lowest value with −232.02 Kcal mol^{-1}, indicating that this free energy is still in good agreement with experimentally reported data (Liu et al., 2020).

Although the values are overestimated regarding the complete systems, the simplified models show the necessary tendency to select higher affinity antibodies at the expense of the precision in the ΔΔG values (Tables 2 and 3). The structural data derived from molecular dynamics and endpoint free energy calculations showed a positive correlation between complete and simplified models (0.82 Pearson correlation coefficient; $t = 3.661$, df = 3, p-value = 0.03522, with a 95% confident interval), suggesting that simplified models reproduce the behavior of complete ectodomain (Figure 5).

3.3. Residue contribution and decomposition analysis of the antigen/antibody interactions

MM/GBSA residue decomposition analysis was performed for the simplified models to identify the contribution of each residue at the interface between SP2 and the different Fabs. Experimentally, two charged lysine residues control the complex formation with the antibody through electrostatic interactions with its side chains, as well as a tyrosine residue that forms a hydrogen bond in the SP-2 – Fab 3022 complex (Table 3). Moreover, for the lowest energy and more stable SP-2 – Fab S-2-4 complex, the interfacial interactions are controlled mainly by electrostatic attractions between charged acidic residues. However, hydrogen bonds imposed by hydroxyl groups to the main antibody chain reduce the desolvation energy term (Table 3).

Our data showed that the electrostatic interactions imposed by Lys378 and Lys386 of the RBD domain of SP-2 are the most important interactions with the lowest energy terms; since Lys378 and Lys386 interact with aspartic acid residues of Fab 3022 (Figure 6A). In the complete model of SP2, Lys378 and Lys386 also possess the lowest energy values indicating that these amino acids play essential roles in the interaction with this antibody. Tyr380 residue formed a hydrogen bond with the main chain of threonine residues from the Fab and surrounding water molecules (Figure 6B). Although the most predominant interactions in the other replicas were those imposed by NH_3^+ of Lys386 residue towards acidic residues on the surface of Fab 3022, there was an exchange for Lys378 at various times of the simulations. Because the 6YOR crystal model does not contain more atoms of SP-2, it is expected that repulsive interactions with the other domains play an essential role in the binding process.

The SP-2 – Fab S-2-4 simulations showed the formation of a bonding interface between a negatively charged patch composed of acidic residues from SP-2 RBD and the side chain of arginine residues from Fab S-2-4. This interaction is predominant along simulation time and comprises the interactions with more negative free energies (Figure 6C). Moreover, the formation of hydrogen bonds with positively charged residues as Arg403, Lys417, and Arg457, contributed to stabilizing the antibody upon RBD. Surprisingly, Tyr380 plays a significant role in forming antigen/antibody interface, forming hydrogen bonds with the main chain of Fab S-2-4 during 63% of the simulation time, and SP-2 – Fab 3022 system (Figure 6D). In the case of the complete system, Lys417 also possesses the main energetic contribution in this complex. However, other amino acids like Tyr380, Asp405, and Arg457 become more energetically predominant residues in this system than in the simplified model. Throughout these experiments, we observed behaviors and trends in the results that could mean an analysis guide to study the behavior of antigen/antibody interfaces. As shown in the residue decomposition analysis, the study region comprises the amino acids that are the most important for antibody-antigen binding.

Since the pandemic persists and the number of variants increases, the demand for new, sensitive, and portable detection techniques is necessary. This theoretical approach presents an alternative methodology for further COVID-19 studies. Since our simplified method is based on the dynamic modeling of few atoms, compared to the whole protein structure, it can be used for quick selection of new high-affinity antibodies, chemical molecules (drug design), or even in the biosensor field (Cerofolini et al., 2020; Eissa & Zourob, 2021). shows a feasible biosensor design taking advantage of the information obtained by the Fab S-2-4 simulations; further explanation of this perspective can be found in the supporting material.

4. Conclusions

The presented methodology is based on accelerated molecular dynamics for structural and energetic characterization of the binding event between SP-2 RBD and different available antibody structures. This method is not limited to available experimental structures since homology models of antibodies can also be analyzed, a valuable tool against the new SARS-CoV-2 variants outbreak. Despite the valuable information that can be obtained from molecular dynamics of biomolecular systems, like the energy involved in ligand-receptor interactions; some limitations need to be addressed: first, the computational cost required in routine simulations greater than dozens of microseconds in length usually leads to an inadequate sampling of conformational states. Also, the high number of particles is often limiting for adequate sampling of the chemical space. Moreover, if we consider the high mutation rate of the virus, routinely simulations of whole new virus variants result in a very demanding approach. The real benefit of this methodology was saving several months of computational time and a lot of computational resources by simplifying the models from millions to thousands of atoms.

Funding

This work was supported by the [CONACYT] under Grant [A1-S-15877] and [PAPIIT-DGAPA-UNAM] under Grant [IN104621]. The authors are grateful for access to computational resources on the Miztli supercomputer through the project UNAM-DGTIC-COVID19-009 and UNAM-DGTIC-347; also an acknowledgment to Centro Nacional de Supercomputo-IPICyT, A.C. (National Supercomputing Center-CNS) for facilities at Thubat-Kaal 2 supercomputer. Special thanks to Engineer Irving Álvarez at DGTIC-UNAM; Engineer Jesús Alaniz at ThubatKaal 2.0 at CNS and MSc. Aldo Rodríguez at CNyN-UNAM for their technical support. A. Vidal-Limon and G.A. Huerta-Miranda thank CONACYT A1-S-15877 for the financial support of their research internship. W.I. García-García thanks the PhD scholarship granted by CONACYT.

ORCID

G. A. Huerta-Miranda http://orcid.org/0000-0003-1183-3668
W. I. García-García http://orcid.org/0000-0001-6503-4103
A. Vidal-Limon http://orcid.org/0000-0001-5674-7881
M. Miranda-Hernández http://orcid.org/0000-0002-6769-4102

Data and software availability

A listing of available data, construction and execution scripts and input structures files are available on the **figshare repository:** 10.6084/m9.figshare.15026352

All the third-party software used in this work is stated in the 'Methods and computational tools' section of the Manuscript. Here is a list of used software: Schrödinger Maestro v. 2019-4; Amber18 CUDA version software (Fee Waiver License for Abraham Vidal-Limon); R Statistical package v. 4.0.1, and CHARMM-GUI server was used for recover of SARS-Cov-2 spike protein full model (https://charmm-gui.org/).

Author contributions

Guillermo A. Huerta Miranda: Formal writing, Reviewing and Editing, Visualization, Investigation.: Wendy I. García-García: Reviewing and Editing, Investigation Writing – Original draft preparation.: Abraham Vidal-Limon: Conceptualization, Methodology, Writing – Original draft preparation.: Margarita Miranda-Hernández: Supervision, Project administration.

Disclosure statement

No potential conflict of interest was reported by the authors.

References

Barnes, C. O., West, A. P., Huey-Tubman, K. E., Hoffmann, M. A. G., Sharaf, N. G., Hoffman, P. R., Koranda, N., Gristick, H. B., Gaebler, C., Muecksch, F., Lorenzi, J. C. C., Finkin, S., Hägglöf, T., Hurley, A., Millard, K. G., Weisblum, Y., Schmidt, F., Hatziioannou, T., Bieniasz, P. D., … Bjorkman, P. J. (2020). Structures of human antibodies bound to SARS-CoV-2 spike reveal common epitopes and recurrent features of antibodies. *Cell*, *182*(4), 828–842.e16. https://doi.org/10.1016/j.cell.2020.06.025

Bicudo, N., Bicudo, E., Costa, J. D., Castro, J. A. L. P., & Barra, G. B. (2020). Co-infection of SARS-CoV-2 and dengue virus: A clinical challenge. *The Brazilian Journal of Infectious Diseases: An Official Publication of the Brazilian Society of Infectious Diseases*, *24*(5), 452–454. https://doi.org/10.1016/j.bjid.2020.07.008

Carter, L. J., Garner, L. V., Smoot, J. W., Li, Y., Zhou, Q., Saveson, C. J., Sasso, J. M., Gregg, A. C., Soares, D. J., Beskid, T. R., Jervey, S. R., & Liu, C. (2020). Assay techniques and test development for COVID-19 diagnosis. *ACS Central Science*, *6*(5), 591–605. https://doi.org/10.1021/acscentsci.0c00501

Casalino, L., Dommer, A. C., Gaieb, Z., Barros, E. P., Sztain, T., Ahn, S.-H., Trifan, A., Brace, A., Bogetti, A. T., Clyde, A., Ma, H., Lee, H., Turilli, M., Khalid, S., Chong, L. T., Simmerling, C., Hardy, D. J., Maia, J. D., Phillips, J. C., … Amaro, R. E. (2021). AI-driven multiscale simulations illuminate mechanisms of SARS-CoV-2 spike dynamics. *The International Journal of High Performance Computing Applications*, *35*(5), 432–451. https://doi.org/10.1177/10943420211006452

Case, D. A., Walker, R. C., Cheatham, T. E., Simmerling, C., Roitberg, A., Merz, K. M., Luo, R., & Darden, T. (2018). *Amber 18*. University of California.

Cerofolini, L., Fragai, M., Luchinat, C., & Ravera, E. (2020). Orientation of immobilized antigens on common surfaces by a simple computational model: Exposition of SARS-CoV-2 Spike protein RBD epitopes. *Biophysical Chemistry*, *265*, 106441 https://doi.org/10.1016/j.bpc.2020.106441

Chu, D. K. W., Pan, Y., Cheng, S. M. S., Hui, K. P. Y., Krishnan, P., Liu, Y., Ng, D. Y. M., Wan, C. K. C., Yang, P., Wang, Q., Peiris, M., & Poon, L. L. M. (2020). Molecular diagnosis of a novel coronavirus (2019-nCoV) causing an outbreak of pneumonia. *Clinical Chemistry*, *66*(4), 549–555. https://doi.org/10.1093/clinchem/hvaa029

Corman, V. M., Landt, O., Kaiser, M., Molenkamp, R., Meijer, A., Chu, D. K., Bleicker, T., Brünink, S., Schneider, J., Schmidt, M. L., Mulders, D. G., Haagmans, B. L., van der Veer, B., van den Brink, S., Wijsman, L., Goderski, G., Romette, J.-L., Ellis, J., Zambon, M., … Drosten, C. (2020). Detection of 2019 novel coronavirus (2019-nCoV) by real-time RT-PCR. *Eurosurveillance*, *25*(3), 23-30. https://doi.org/10.2807/1560-7917.ES.2020.25.3.2000045

Eissa, S., & Zourob, M. (2021). Development of a Low-Cost Cotton-Tipped Electrochemical Immunosensor for the Detection of SARS-CoV-2. *Analytical Chemistry*, *93*(3), 1826–1833. https://doi.org/10.1021/acs.analchem.0c04719

Forssen, P., Samuelsson, J., Lacki, K., & Fornstedt, T. (2020). Advanced analysis of biosensor data for SARS-COV-2 RBD and ACE2 interactions. *Analytical Chemistry*, *92*(17), 11520–11524. https://doi.org/10.1021/acs.analchem.0c02475

Garcia-Garcia, W. I., Vidal-Limon, A., Arrocha-Arcos, A. A., Palomares, L. A., Ramirez, O. T., & Miranda-Hernández, M. (2019). Rotavirus VP6 protein as a bio-electrochemical scaffold: Molecular dynamics and experimental electrochemistry. *Bioelectrochemistry (Amsterdam, Netherlands)*, *127*, 180–186. https://doi.org/10.1016/j.bioelechem.2019.02.012

Genheden, S., & Ryde, U. (2012). Comparison of end-point continuum-solvation methods for the calculation of protein-ligand binding free energies. *Proteins*, *80*(5), 1326–1342. https://doi.org/10.1002/prot.24029

Genheden, S., & Ryde, U. (2015). The MM/PBSA and MM/GBSA methods to estimate ligand-binding affinities. *Expert Opinion on Drug Discovery*, *10*(5), 449–461. https://doi.org/10.1517/17460441.2015.1032936

Henrina, J., Putra, I. C. S., Lawrensia, S., Handoyono, Q. F., & Cahyadi, A. (2020). Coronavirus disease of 2019: A mimicker of dengue infection? *SN Comprehensive Clinical Medicine*, *2*(8), 1109–1119. https://doi.org/10.1007/s42399-020-00364-3

Hoffmann, M., Kleine-Weber, H., Schroeder, S., Krüger, N., Herrler, T., Erichsen, S., Schiergens, T. S., Herrler, G., Wu, N. H., Nitsche, A., Müller, M. A., Drosten, C., & Pöhlmann, S. (2020). SARS-CoV-2 cell entry depends on ACE2 and TMPRSS2 and is blocked by a clinically proven protease inhibitor. *Cell*, *181*(2), 271–280.e8. https://doi.org/10.1016/j.cell.2020.02.052

Huo, J., Zhao, Y., Ren, J., Zhou, D., Duyvesteyn, H. M. E., Ginn, H. M., Carrique, L., Malinauskas, T., Ruza, R. R., Shah, P. N. M., Tan, T. K., Rijal, P., Coombes, N., Bewley, K. R., Tree, J. A., Radecke, J., Paterson, N. G., Supasa, P., Mongkolsapaya, J., … Stuart, D. I. (2020). Neutralization of SARS-CoV-2 by destruction of the prefusion spike. *Cell Host & Microbe*, *28*(3), 445–454.e6. https://doi.org/10.1016/j.chom.2020.06.010

Jarocka, U., Sawicka, R., Góra-Sochacka, A., Sirko, A., Zagórski-Ostoja, W., Radecki, J., & Radecka, H. (2014). An immunosensor based on antibody binding fragments attached to gold nanoparticles for the detection of peptides derived from avian influenza hemagglutinin H5. *Sensors (Basel, Switzerland)*, *14*(9), 15714–15728. https://doi.org/10.3390/s140915714

Jo, S., Kim, T., Iyer, V. G., & Im, W. (2008). CHARMM-GUI: A web-based graphical user interface for CHARMM. *Journal of Computational Chemistry*, *29*(11), 1859–1865. https://doi.org/10.1002/jcc.20945

Ju, B., Zhang, Q., Ge, J., Wang, R., Sun, J., Ge, X., Yu, J., Shan, S., Zhou, B., Song, S., Tang, X., Yu, J., Lan, J., Yuan, J., Wang, H., Zhao, J., Zhang, S., Wang, Y., Shi, X., … Zhang, L. (2020). Human neutralizing antibodies elicited by SARS-CoV-2 infection. *Nature*, *584*(7819), 115–119. https://doi.org/10.1038/s41586-020-2380-z

Liu, L., Wang, P., Nair, M. S., Yu, J., Rapp, M., Wang, Q., Luo, Y., Chan, J. F.-W., Sahi, V., Figueroa, A., Guo, X. V., Cerutti, G., Bimela, J., Gorman, J., Zhou, T., Chen, Z., Yuen, K.-Y., Kwong, P. D., Sodroski, J. G., … Ho, D. D. (2020). Potent neutralizing antibodies against multiple epitopes on SARS-CoV-2 spike. *Nature*, *584*(7821), 450–456. https://doi.org/10.1038/s41586-020-2571-7

Lustig, Y., Keler, S., Kolodny, R., Ben-Tal, N., Atias-Varon, D., Shlush, E., Gerlic, M., Munitz, A., Doolman, R., Asraf, K., Shlush, L. I., & Vivante, A. (2021). Potential antigenic cross-reactivity between severe acute respiratory syndrome coronavirus 2 (SARS-CoV-2) and dengue viruses. *Clinical Infectious Diseases : An Official Publication of the Infectious Diseases Society of America*, *73*(7), e2444–e2449. https://doi.org/10.1093/cid/ciaa1207

Masyeni, S., Santoso, M. S., Widyaningsih, P. D., Asmara, D. G. W., Nainu, F., Harapan, H., & Sasmono, R. T. (2021). Serological cross-reaction and coinfection of dengue and COVID-19 in Asia: Experience from Indonesia. *International Journal of Infectious Diseases*, *102*, 152–154. https://doi.org/10.1016/j.ijid.2020.10.043

Miao, Y., Feher, V. A., & McCammon, J. A. (2015). Gaussian accelerated molecular dynamics: Unconstrained enhanced sampling and free energy calculation. *Journal of Chemical Theory and Computation*, *11*(8), 3584–3595. https://doi.org/10.1021/acs.jctc.5b00436

Miao, Y., & McCammon, J. A. (2017). Gaussian accelerated molecular dynamics: Theory, implementation, and applications. *Annual Reports in Computational Chemistry*, *13*, 231–278. https://doi.org/10.1016/bs.arcc.2017.06.005

Olsson, M. H. M., Søndergaard, C. R., Rostkowski, M., & Jensen, J. H. (2011). PROPKA3: Consistent treatment of internal and surface residues in empirical pKa predictions. *Journal of Chemical Theory and Computation*, *7*(2), 525–537. https://doi.org/10.1021/ct100578z

Pinto, D., Park, Y.-J., Beltramello, M., Walls, A. C., Tortorici, M. A., Bianchi, S., Jaconi, S., Culap, K., Zatta, F., De Marco, A., Peter, A., Guarino, B., Spreafico, R., Cameroni, E., Case, J. B., Chen, R. E., Havenar-Daughton, C., Snell, G., Telenti, A., … Corti, D. (2020). Cross-neutralization of SARS-CoV-2 by a human monoclonal SARS-CoV antibody. *Nature*, *583*(7815), 290–295. https://doi.org/10.1038/s41586-020-2349-y

Planas, D., Veyer, D., Baidaliuk, A., Staropoli, I., Guivel-Benhassine, F., Rajah, M. M., Planchais, C., Porrot, F., Robillard, N., Puech, J., Prot, M., Gallais, F., Gantner, P., Velay, A., Le Guen, J., Kassis-Chikhani, N., Edriss, D., Belec, L., Seve, A., … Schwartz, O. (2021). Reduced sensitivity of SARS-CoV-2 variant Delta to antibody neutralization. *Nature*, *596*(7871), 276–280. https://doi.org/10.1038/s41586-021-03777-9

Quental, K. N., Leite, A. L., Feitosa, A., do, N. A., Oliveira, Z. N. P., de, Tavares, L. V., de, S., Tavares, W. G., de, S., Pinheiro, E. F., Lacsina, J. R., DeSouza-Vieira, T., & Silva, J. B. N. F. (2021). SARS-CoV-2 co-infection with dengue virus in Brazil: A potential case of viral transmission by a health care provider to household members. *Travel Medicine and Infectious Disease*, *40*, 101975. https://doi.org/10.1016/j.tmaid.2021.101975

Roe, D. R., & Cheatham, T. E. (2013). PTRAJ and CPPTRAJ: Software for processing and analysis of molecular dynamics trajectory data. *Journal of Chemical Theory and Computation*, *9*(7), 3084–3095. https://doi.org/10.1021/ct400341p

Santoso, M. S., Masyeni, S., Haryanto, S., Yohan, B., Hibberd, M. L., & Sasmono, R. T. (2021). Assessment of dengue and COVID-19 antibody rapid diagnostic tests cross-reactivity in Indonesia. *Virology Journal*, *18*(1), 54.https://doi.org/10.1186/s12985-021-01522-2

Souza, P. F. N., Lopes, F. E. S., Amaral, J. L., Freitas, C. D. T., & Oliveira, J. T. A. (2020). A molecular docking study revealed that synthetic peptides induced conformational changes in the structure of SARS-CoV-2 spike glycoprotein, disrupting the interaction with human ACE2 receptor. *International Journal of Biological Macromolecules*, *164*, 66–76. https://doi.org/10.1016/j.ijbiomac.2020.07.174

Urban, G. A. (2000). Biosensor design and fabrication. *Encyclopedia of Analytical Chemistry*, *2*, 1164–1181. https://doi.org/10.1002/9780470027318.a0505

Vidal-Limon, A., Antonio Huerta-Miranda, G., I., García-García, W., & Miranda-Hernández, M. (2021). Design of bioelectrochemical interfaces assisted by molecular dynamics simulations. In *Homology molecular modeling—Perspectives and applications* (pp. 1–18). IntechOpen. https://doi.org/10.5772/intechopen.93884

Walls, A. C., Park, Y.-J., Tortorici, M. A., Wall, A., McGuire, A. T., & Veesler, D. (2020). Structure, function, and antigenicity of the SARS-CoV-2 spike glycoprotein. *Cell*, *181*(2), 281–292.e6. https://doi.org/10.1016/j.cell.2020.02.058

Walls, A. C., Xiong, X., Park, Y.-J., Tortorici, M. A., Snijder, J., Quispe, J., Cameroni, E., Gopal, R., Dai, M., Lanzavecchia, A., Zambon, M., Rey, F. A., Corti, D., & Veesler, D. (2019). Unexpected receptor functional mimicry elucidates activation of coronavirus fusion. *Cell*, *176*(5), 1026–1039.e15. https://doi.org/10.1016/j.cell.2018.12.028

Wang, C., Horby, P. W., Hayden, F. G., & Gao, G. F. (2020). A novel coronavirus outbreak of global health concern. *The Lancet*, *395*(10223), 470–473. https://doi.org/10.1016/S0140-6736(20)30185–9

Wang, Q., Zhang, Y., Wu, L., Niu, S., Song, C., Zhang, Z., Lu, G., Qiao, C., Hu, Y., Yuen, K. Y., Wang, Q., Zhou, H., Yan, J., & Qi, J. (2020). Structural and functional basis of SARS-CoV-2 entry by using human ACE2. *Cell*, *181*(4), 894–904.e9. https://doi.org/10.1016/j.cell.2020.03.045

Won, J., Lee, S., Park, M., Kim, T. Y., Park, M. G., Choi, B. Y., Kim, D., Chang, H., Kim, V. N., & Lee, C. J. (2020). Development of a laboratory-safe and low-cost detection protocol for SARS-CoV-2 of the coronavirus disease 2019 (COVID-19). *Experimental Neurobiology*, *29*(2), 107–119. https://doi.org/10.5607/en20009

Woo, H., Park, S.-J., Choi, Y. K., Park, T., Tanveer, M., Cao, Y., Kern, N. R., Lee, J., Yeom, M. S., Croll, T. I., Seok, C., & Im, W. (2020). Developing a fully glycosylated full-length SARS-CoV-2 spike protein model in a viral membrane. *The Journal of Physical Chemistry. B*, *124*(33), 7128–7137. https://doi.org/10.1021/acs.jpcb.0c04553

World Health Organization. (2020). *WHO coronavirus disease (COVID-19) dashboard*. World Health Organization.

Wrapp, D., Wang, N., Corbett, K. S., Goldsmith, J. A., Hsieh, C. L., Abiona, O., Graham, B. S., & McLellan, J. S. (2020). Cryo-EM structure of the 2019-nCoV spike in the prefusion conformation. *Science*, *367*(6483), 1260–1263. https://doi.org/10.1126/science.abb2507

Zhou, P., Yang, X.-L., Wang, X.-G., Hu, B., Zhang, L., Zhang, W., Si, H.-R., Zhu, Y., Li, B., Huang, C.-L., Chen, H.-D., Chen, J., Luo, Y., Guo, H., Jiang, R.-D., Liu, M.-Q., Chen, Y., Shen, X.-R., Wang, X., … Shi, Z.-L. (2020a). A pneumonia outbreak associated with a new coronavirus of probable bat origin. *Nature*, *588*(7836), E6–E6. https://doi.org/10.1038/s41586-020-2012-7

Zhou, P., Yang, X.-L., Wang, X.-G., Hu, B., Zhang, L., Zhang, W., Si, H.-R., Zhu, Y., Li, B., Huang, C.-L., Chen, H.-D., Chen, J., Luo, Y., Guo, H., Jiang, R.-D., Liu, M.-Q., Chen, Y., Shen, X.-R., Wang, X., … Shi, Z.-L. (2020b). A pneumonia outbreak associated with a new coronavirus of probable bat origin. *Nature*, *579*(7798), 270–273. https://doi.org/10.1038/s41586-020-2012-7

Zhu, X., Wang, X., Han, L., Chen, T., Wang, L., Li, H., Li, S., He, L., Fu, X., Chen, S., Xing, M., Chen, H., & Wang, Y. (2020). Multiplex reverse transcription loop-mediated isothermal amplification combined with nanoparticle-based lateral flow biosensor for the diagnosis of COVID-19. *Biosensors and Bioelectronics*, *166*, 112437. https://doi.org/10.1016/j.bios.2020.112437

Zuo, X., Fan, C., & Chen, H.-Y. (2017). Biosensing: CRISPR-powered diagnostics. *Nature Biomedical Engineering*, *1*(6), 91. https://doi.org/10.1038/s41551-017-0091